ELSEVIER

Journal of Hazardous Materials 57 (1998) 79–103

JOURNAL OF HAZARDOUS MATERIALS

Negative buoyancy effects on the dispersion of continuous gas plumes downwind solid obstacles

Michel Ayrault [a,*], Serge Simoëns [a], Patrick Méjean [b]

[a] *Laboratoire de Mécanique des Fluides et d'Acoustique, UMR 5509 CNRS, Ecole Centrale de Lyon, BP 163, Ecully 69131, Cedex, France*

[b] *Société METRAFLU, 64 Chemin des Mouilles, Ecully 69134, Cedex, France*

Received 22 July 1996; accepted 29 May 1997

Abstract

An investigation of continuous dense gas plumes released from a surface area source and dispersing downwind solid obstacles is presented. Comparison with passive plumes released in the same experimental conditions enables us to emphasize the buoyancy effects. Some quantitative statistical results such as mean concentration, root-mean-square fluctuations, skewness and kurtosis are given. The experimental technique used, visualizations and digital image processing, allows us to characterize the geometrical evolution of the plumes. © 1998 Elsevier Science B.V.

Keywords: Negative buoyancy; Gas plumes; Solid obstacles

1. Introduction

Dispersion of heavier than air gases in the atmosphere has been particularly studied with respect to accidental releases of hazardous materials. When released in the atmosphere, they generally produce clouds denser than the environment [1–4]. The evolution of such negatively buoyant clouds is quite different from passive or positively buoyant plumes. Due to the negative buoyancy, they cover a large surface area with a limited vertical depth. Furthermore, they are very sensitive to the effects of man-made or natural obstacles which influence strongly the dispersion, the influence of obstacles being greater for heavy clouds than neutral.

The inertia of released materials is directly dependent upon the density. The influence could be most important close to the source where the density difference is large. The

* Corresponding author.

PII S0304-3894(97)00075-7

density variation in the vertical direction will be stably stratified so that turbulence and turbulent mixing can be significantly reduced.

The greatest effects of plume stability are the reduction of the plume depth, the depth decreasing with increasing the density effects, an increase of the width and the plume lateral dispersion which is strongly affected by stability. The horizontal density difference produces an additional transport mechanism to that provided by the ambient flow so that the lateral growth of a dense cloud results from both the boundary layer turbulence and the buoyancy driven flow which is essentially deterministic.

For a dense plume spreading under a turbulent flow, the near source region may involve both an inertial interaction and a scouring of the fluid near the source by the ambient flow. The plume can extend upwind of the source and can be wider than the physical source size at the source position. This can influence both obstacle and shear stress effects. In order to quantify and predict these effects, one can define different buoyancy flow parameters. For example, as noted by Britter and McQuaid [5], the parameter

$$\sqrt[3]{\frac{g'_0 q_0}{\Phi_s U_\infty^3}}$$

exhibits the influence of the external velocity on the release, $g'_0 = g[(\rho_0 - \rho_a)/(U_\infty^3)]$ represents the modified gravity with ρ_0 and ρ_a the initial density of the cloud and of the ambient fluid, respectively, q_0 the volumetric gas release rate, Φ_s the source diameter and U_∞ the external mean velocity. A value smaller than 0.15 indicates a release behavior identical to a passive plume. Parameters characterizing the effects of stability could also be introduced [6] as a buoyancy-driven length scale $L_b = (g'_0 q_0)/(U_\infty^3)$ and a buoyancy parameter

$$B = g'_0 \sqrt{\frac{q_0}{u_*^5}} .$$

The length L_b characterizes the physical source size effect, whereas, the buoyancy flux parameter B describes the plume behavior. Small values of L_b indicate a predominance of the physical source size and large values of B, an increase of the lateral spreading, the vertical dispersion being reduced. A rapid collapse to the ground of the discharged plume with limited dispersion around the source is noted and the mainstream flow is deflected over the release rather than mixed with the dense gas.

An approximate indicator of the relative plume rise of the source discharge due to its momentum is given by the momentum flux parameter

$$M = \frac{w_s}{u_*} \sqrt{\frac{\rho_0}{\rho_a}} \text{ [4]}, \; w_s$$

being the gas source velocity, values lower than 0.2 indicating negligible source momentum. However, for very high values, the source discharge momentum effects also become negligible which are amplified by the negative buoyancy of plumes. The effects of the source discharge momentum are suppressed by the negative buoyancy because the very high values of B diminish the great sensitivity to the discharge momentum.

The understanding of such dense gas clouds behavior is a result of various types of experiments, field or laboratory experiments.

Fields experiments generally consider more realistic scenarios, less idealized sources at scales of a possible accidental release where liquefied gas are realized as ammonia or hydrogen fluoride. We can note some important field experiments, China Lake LNG trials (1980–1983), Nevada desert trials (1983) and Thorney Island heavy gas experiments (1980–1983). Unfortunately, these experiments which require extensive instrumentation and are always expensive are generally difficult to analyze due to the great variability of the atmospheric external conditions. It is always possible to use laboratory experiments to simulate such accidental releases but one need to keep in mind that only approximate similarity is realizable, both in wind tunnel or water channel.

On the other hand, one can also devise idealized laboratory experiments to study specific phenomena, specific physical processes (no more than one or two) which allows a detailed investigation and quantification of these processes. Such experiments as two-dimensional plumes or continuous plumes from an area source over flat terrain are far from realistic scenarios. One can see, for example, Hall and Waters [7] for an experimental study of the effects of source size on plume dispersion and the transition between the neutrally buoyant state to that of a clearly heavier than air plume and Schatzmann et al. [8] for heavy gas jets in laminar and turbulent cross-flows. A review of the main experiments about dense gas dispersion can be found in the paper of Builtjes [9] and Britter (in Ref. [1]).

In many situations, the dispersion of accidentally released heavy gas plumes or jets is influenced by obstacles located at the vicinity of the source. The main effects of obstacles on a dense plume will be to divert the flow, to increase mixing and dilute the plume if there is no channelling effect. Some idealized works have been performed on the effects of obstacles on the dispersion, Sutton et al. [10] and Britter [6]. Britter, for example, study the impingement of a 2D plume and an area source plume on 2D and 3D obstacles. Many other different studies can be found in the Fladis final report [11], the effects of two-dimensional solid fences and buildings on dispersion of heavy plumes or jets, the transition of near field heavy gas dispersion to far field passive gas dispersion and the effect of release duration on dispersion.

It is evident that the density difference $(\rho - \rho_a)/(\rho_a)$, where ρ and ρ_a are the density of the cloud and of the ambient fluid, respectively, is not the only variable determining whether or not the plume behaves as a dense cloud. We also note important effects and a great interaction between the different buoyancy parameters, the external turbulent flow characteristics, the initial release conditions such as source size, shape and discharge momentum. In the presence of obstacles, specific geometries such as two- or three-dimensional obstacles, their heights, the ratio between the height obstacle and the plume depth without obstacle or the angle with the mean flow influence dispersion downwind the obstacles. All this call for considerable caution in the interpretation of results and in the development of physical models.

The experiments described here concern an idealized situation of the dispersion of continuous dense gas plumes released from a circular source flush with the floor over some two-dimensional or semi-circular solid fences. The experimental technique combines visualizations and digital image processing. Both neutrally buoyant (passive) and

negatively buoyant (dense) gases were used so that the specific effects of the density difference (a flat wide plume downwind of the source) could be observed downwind the fences, in the recirculating bubbles and in the near wakes. Comparison with the dispersion on flat terrain clearly shows the effects of the obstacles on the dispersion.

2. Experimental technique and facilities

The experiments were carried out in the EDF-ECL atmospheric wind-tunnel. A neutrally stratified boundary layer on flat floor was obtained by using a porous fence at the entrance of the wind-tunnel section. In the equilibrium section, the Reynolds number $R_e = (U_\infty \delta)/(\upsilon)$ was about 10^4, the external velocity $U_\infty = 1$ m s^{-1}, the boundary layer thickness $\delta = 0.18$ m, the friction velocity $u_* = 0.044$ m s^{-1} and the ground roughness length $z_0 = 0.2$ mm. Fig. 1 shows mean velocity and longitudinal root-mean-square fluctuations profiles in the equilibrium section situated 7.4 m downwind the test section entrance. This section corresponds to the center of the ground area source for the continuous plumes studied.

The area source was circular, 50-mm diameter and flush with the wind-tunnel floor in the equilibrium section. The volumetric gas release rate was constant for the different plumes studied, $q_0 = 183 \times 10^{-6}$ m^3 s^{-1} and the source gas discharge velocity, averaged over the whole source area was $w_s = 0.10$ m s^{-1}. For the dense gas considered, the density was 2.1, the modified gravity 10.8 m s^{-2} and the buoyancy flux parameter $g'_0 q_0$ about 2×10^{-3} m^4 s^{-3}. Two-dimensional thin solid fences of heights 30 and 60 mm were fixed on the tunnel floor and set normal to the mean wind-tunnel flow at 0.4 m downstream from the source center (i.e. 8 source diameters). A semi-circular solid fence of height 30 mm was also studied, the center of the fence corresponding to the area

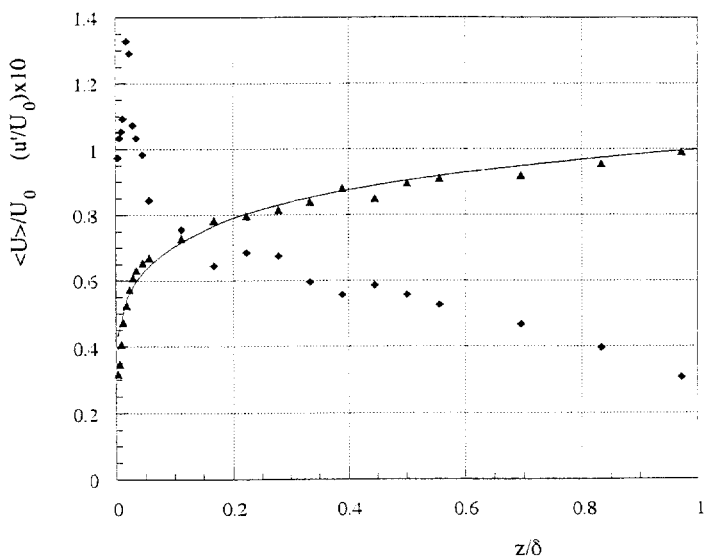

Fig. 1. Mean (triangles) and r.m.s. fluctuations (squares) vertical velocity profiles on flat floor at the center of the release (r.m.s. values are multiplied by a factor 10). The straight curve represents the power law in 1/7.

source center. A schematic plan view of plumes and fences, as described above, is given on Fig. 2a. The center of the source corresponds to the origin of the geometrical axes *OXYZ*, *OX* being the longitudinal axis and *OZ* the vertical.

Laser tomography visualizations were made in two different planes, a vertical plane on the longitudinal axis ($y = 0$) and a horizontal plane situated 8 mm above the floor (Fig. 2b). The 2-mm thick light plane was generated by a 5-W argon laser beam deflected by a set of 12 rotating mirrors. As depicted on the Fig. 2b, the laser beam was sweeping the flow region of interest, the mirror's rotation frequency was set to 50 Hz. Before being released into the flow, the dense gas was seeded with fine particles of

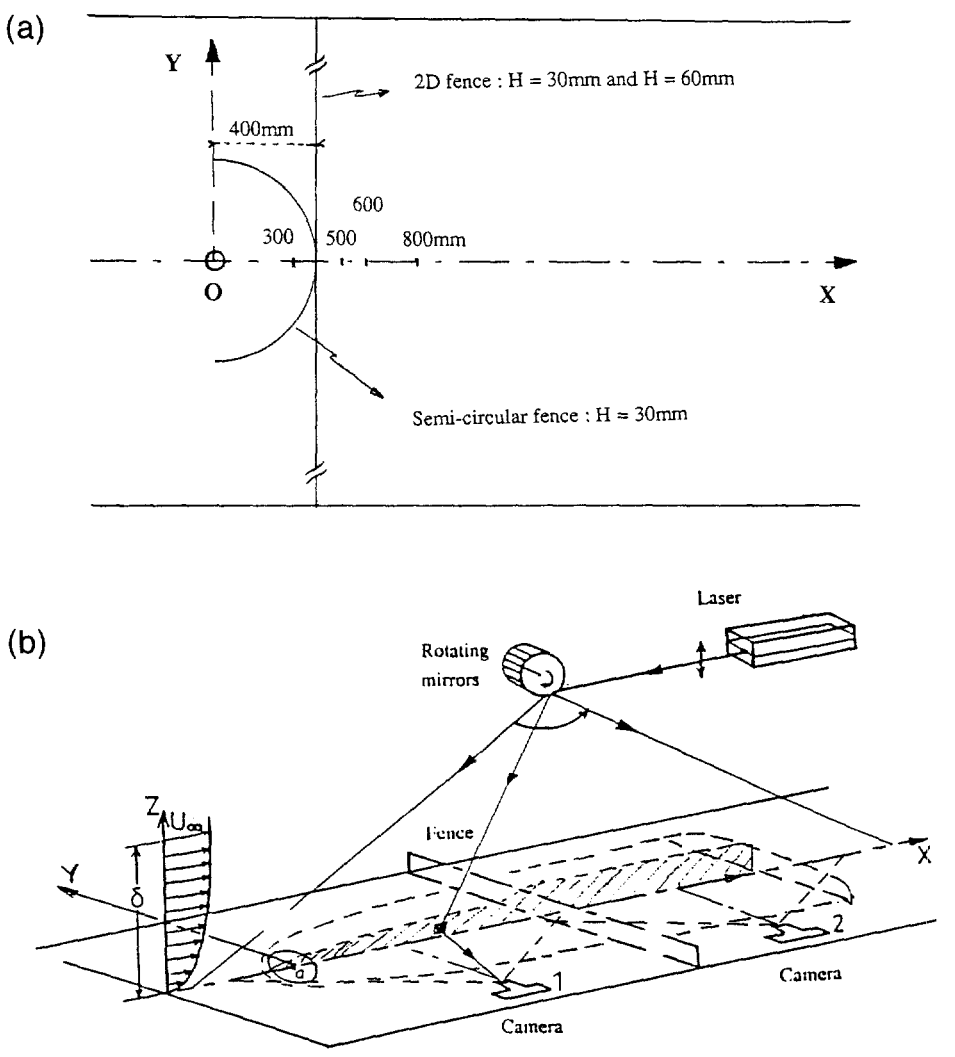

Fig. 2. (a) Schematic plane view of the source and the different fences. (b) Experimental set-up.

incense, the mean diameter was 0.8 mm and the standard deviation of 0.2 μm. The volumetric mass ρ_p of these particles is quite greater than that of air ($\rho_p/\rho_a \ll 1$) and from the Basset–Boussinesq–Oseen equation, we can introduce a relaxation time of the particles as

$$\tau_p = \frac{4a^2}{36\mu}(\rho_a + 2\rho_p) \approx \frac{8a^2\rho_p}{36\mu}$$

For incense particles moving in air, with $\rho_p = 0.2 \times 10^{-3}$ kg m^{-3} and $\mu = 16 \times 10^{-2}$ kg s^{-1} m^{-1}, we get

$$\tau_p \approx \frac{8a^2\rho_p}{36\mu} \cong 1.8 \times 10^{-8}\ \text{s}$$

This relaxation time is much smaller than the time scale of dispersion phenomena and we could consider that the particles are following the turbulent flow quite well.

Particles located at any time in the light plane scattered a certain amount of light energy. The scattered light was recorded using one CCD camera for the horizontal sheet and two synchronized CCD cameras for the vertical sheet, images being acquired on two video recorders. The two video cameras were adjusted to operate in linear mode. Upstream the fence the flow was imaged (see Fig. 2b) with the first camera while the second camera imaged the flow downstream where particles were more diluted. The camera aperture (the f# number) was then varied to increase the light reaching the second camera detector. An overlap of some centimeters was used to match the two sets of data after proper rescaling. The video images were then digitized and analyzed for digital analysis purposes. A data set of 250 images was acquired for each experiment. A complete description of this experimental technique with precise relations can be found in the paper of Ayrault and Simoëns [12].

This experimental technique uses solid incense particles for the determination of gas concentration. Ayrault et al. [13] have clearly shown that particles follow the passive or dense gas flow very well and that the light scattering measurements which are proportional to the number of particles present in a given volume provide good measurements of instantaneous gas concentration.

One remark could first be made about using particles for concentration determination. With particles, we can introduce an apparent diffusivity [14] given by

$$D = \left(1 - \frac{\rho_a}{\rho_p}\right)\frac{KT}{6\pi\mu a} \approx \frac{KT}{6\pi\mu a}$$

where K represents the constant of Boltzman and T the absolute temperature. This diffusivity being very small, $D \cong 1.49 \times 10^{-11}$ m s^{-2}, the associate Schmidt number will be very large, $S_c = \nu/D \cong 10^5$. This value should be compare to the diffusion of temperature in air, or more generally to the dispersion of different gases in air, these Schmidt numbers are of the order of magnitude of unity. The main consequence of this characteristic is that no molecular diffusion occurs and particles are only dispersing under the effects of turbulence. This will probably increase the fluctuations of concentration.

For the experiments, the spatial resolution, a function of the observation field, was 1.1 mm for both cameras on the vertical Z axis (for the vertical plane) and 2.4 mm on the two horizontal directions X and Y. By comparison, the turbulent Taylor and Kolmogorov length scales on the vertical direction are respectively $\lambda_z \approx 10$–20 mm and $\eta_z \approx 0.5$–1 mm. Furthermore, the minimum detectable concentration was evaluated to 1% for the first camera and about to 0.1% for the second due to the different camera aperture used.

Finally, we will just note that the particle concentration at any location can only be measured relative to the concentration at other locations. With imaging techniques, we are concerned with ensemble average statistical results, the number of samples corresponding to the number M of digitized images. Let us consider $N_k(x,0,z,t)$ the instantaneous number of particles located at time t in the elemental volume $\mathrm{d}V$ and $Z_c(x,0,z,t)$ the grey level value of the corresponding instantaneous corrected image. If we consider a reference section (subscript $_0$) where the grey level $Z_0(x_0,0,z_0)$ is constant for all the M instantaneous images, the non-dimensionalized mean statistical grey level values are then equal to the non-dimensionalized concentration values and we can write

$$\frac{\frac{1}{M}\sum_k N_k(x,0,z,t)}{\frac{1}{M}\sum_k N_{0k}(x_0,0,z_0)} = \frac{\langle Z_c(x,0,z) - Z_f\rangle}{\langle Z_0(x_0,0,z_0) - Z_f\rangle} = \frac{\langle C(x,0,z)\rangle}{\langle C_0(x_0,0,z_0)\rangle}$$

$$\frac{\frac{1}{M}\sum_k \left[N_k - \left(\frac{1}{M}\sum_k N_k\right)\right]^2}{\left[\frac{1}{M}\sum_k N_{0k}\right]^2} = \frac{\langle z^2(x,0,z)\rangle}{\langle Z_0(x_0,0,z_0) - Z_f\rangle^2} = \frac{\langle c^2(x,0,z)\rangle}{\langle C_0(x_0,0,z_0)\rangle^2}$$

where $\langle C(x,0,z)\rangle$ and $\langle c^2(x,0,z)\rangle$ represent the mean concentration and the variance concentration for the volume $\mathrm{d}V$ centered at the point $(x, y = 0, z)$. The non-dimensionalized mean and turbulent concentration fields are determined with the mean and fluctuant grey level values.

3. Concentration measurements

3.1. General description of dense gas plumes over flat floor

Although we are concerned with the effects of solid fences on the dispersion of continuous releases, we present here some characteristics on flat terrain (more details concerning these experiments may be obtained in Ref. [15]). The different parameters of the dense plumes are listed on Table 1. From their values, far from the critical values where buoyancy could be negligible, we can expect that the buoyancy effects would be quite significant.

Table 1
Experimental initial characteristics of the dense continuous plumes

Modified gravity $g'_0 = g[(\Delta\rho_0)/(\rho_a)]$	10.8 m s^{-2}
Buoyancy flux $g'_0 q_0$	1.98×10^{-3} m^4 s^{-3}
Characteristic lengths $L_b = g'_0 q_0 / U_*^3$	1.98×10^{-3} m
	0.02 m
Characteristic velocity $U_{cc} = [q_0 g'^2_0]^{1/5}$	0.46 m s^{-1}
Characteristic time $T_{cc} = [(q_0)/(g'^3_0)]^{1/5}$	0.043 s
$\sqrt[3]{\frac{g'_0 q_0}{\Phi_s}} / U_*$	0.34
$M = \frac{w_s}{u_*}\sqrt{\frac{\rho_0}{\rho_a}}$	3.1
$B = g'_0\sqrt{\frac{q_0}{u_*}}$	360

The different heights and ground level coverages of instantaneous plumes are quite different as clearly shown on the instantaneous images for passive and dense plumes (see further Fig. 6). An evaluation of the mean widths in the fence section indicates that the width is 2.5 greater for the mean dense plume than for the passive plume. The mean height is 4 times smaller. The aspect ratios of the plume's height h divided by the width W in the fence section ($X = 400$ mm) clearly show the effects of buoyancy and are respectively 0.4 and 0.044 for the passive and dense mean plumes (10 times smaller).

Ground level concentrations downstream from the source on the centerline are similar for both passive and dense plumes and decrease as a power of x^{-1} (Fig. 3). For the greater density 2.1, this power law starts only at $X = 500$ mm downwind the source after a region of transition. This confirms the decrease law established by Britter and Snyder [16] for their passive and dense plumes ($d_0 = 1.52$) up to $X = 1000$ mm. The vertical mean concentration profiles exhibit distinct different shapes for neutral and dense plumes in the different sections and as reported by Britter and Snyder [14], no similarity is noted on the concentration profiles.

On the other hand, the lateral mean concentration profiles for the neutral and dense plumes exhibit completely different profiles. When the ordinate y is normalized by the plume width σ_y and the mean concentration $\langle C(x,0,z)\rangle$ by the maximum of concentration $\langle C(x,0,z)\rangle_{max}$ in the section, passive plumes (Fig. 4a) have gaussian forms in the different sections studied, whereas, the buoyancy effects are clearly seen for the dense plumes (Fig. 4b). These profiles are not flat topped but curved on the release axis, two maxima being attained in the outer regions with sharp tails. In that case, the plume's widths σ_y are considered relative to these maxima. These characteristics are due to the important initial density of the release ($d_0 = 2.1$). When the dense gas is released from the area source, plume causes obstructions to the external flow as a solid obstacle and flow disturbances are generated. As a result of the interaction with the external flow, the mainstream flow is separated over the release rather than mixed with the dense gas and a trailing vortices flow is generated downstream the plume (this typical flow was already

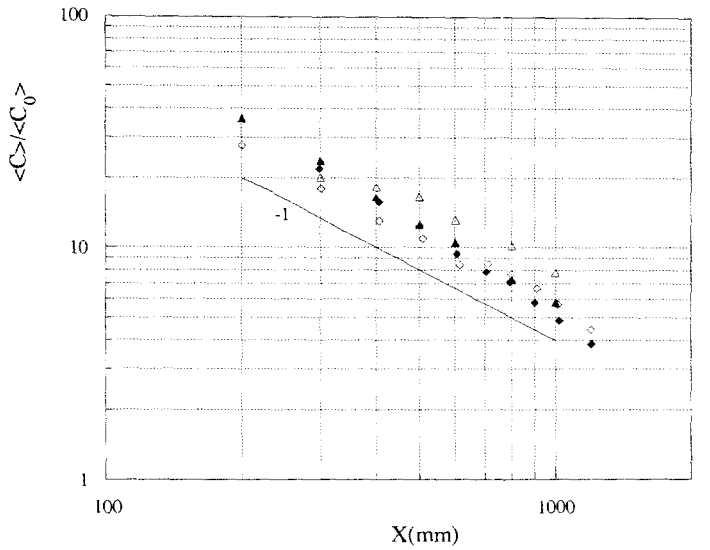

Fig. 3. Longitudinal ground level concentrations decrease versus X for both passive (filled symbols) and dense (open symbols) plumes on flat floor. Triangles refer to our experiments and squares to Britter's experiments (1988).

noted by Hall and Waters [7]). Downstream, the dense plume is nearly split into two secondary plumes which slowly recombine with each other and mix together with some external air. When going downwind, the plumes exhibit a tendency towards the flat topped shape which occurred if the density was smaller. From the normalized profiles, some self-similarity could be expected for both passive and dense plumes.

Concerning the vertical root-mean-square fluctuation profiles, they are all similar for both neutral and dense plumes but concentration fluctuations are reduced when the plume is dense. This fact has already been noted by Stretch [17] and is probably due to the fact that the self generated motion induced inside the cloud by gravity is essentially deterministic, not random. When we plot the r.m.s. values $(\langle c'^2(x,0,z)\rangle)^{1/2}$ normalized by their maxima $(\langle c'^2(x,0,z)\rangle)^{1/2}_{\max}$ versus height normalized by the averaged height h_m, for both passive and dense plumes, we obtain two sets of data which show the same features as shown on Fig. 5. In this flow region, some self-similarity could also be expected.

3.2. General description of dense gas plumes over thin solid obstacles

We briefly describe in this section the flow around thin two-dimensional solid fences, a complete description of these turbulent flows could be found for example in the papers of Counihan et al. [18] and Perera [19]. First of all, two recirculation bubbles exist on each side of the fence. Upstream, a small one starts near the surface at about one height. The other recirculation bubble is located behind the fence, starting at the top of the fence and ending on the surface at a distance between $5H$ to $10H$. In our case, the observed

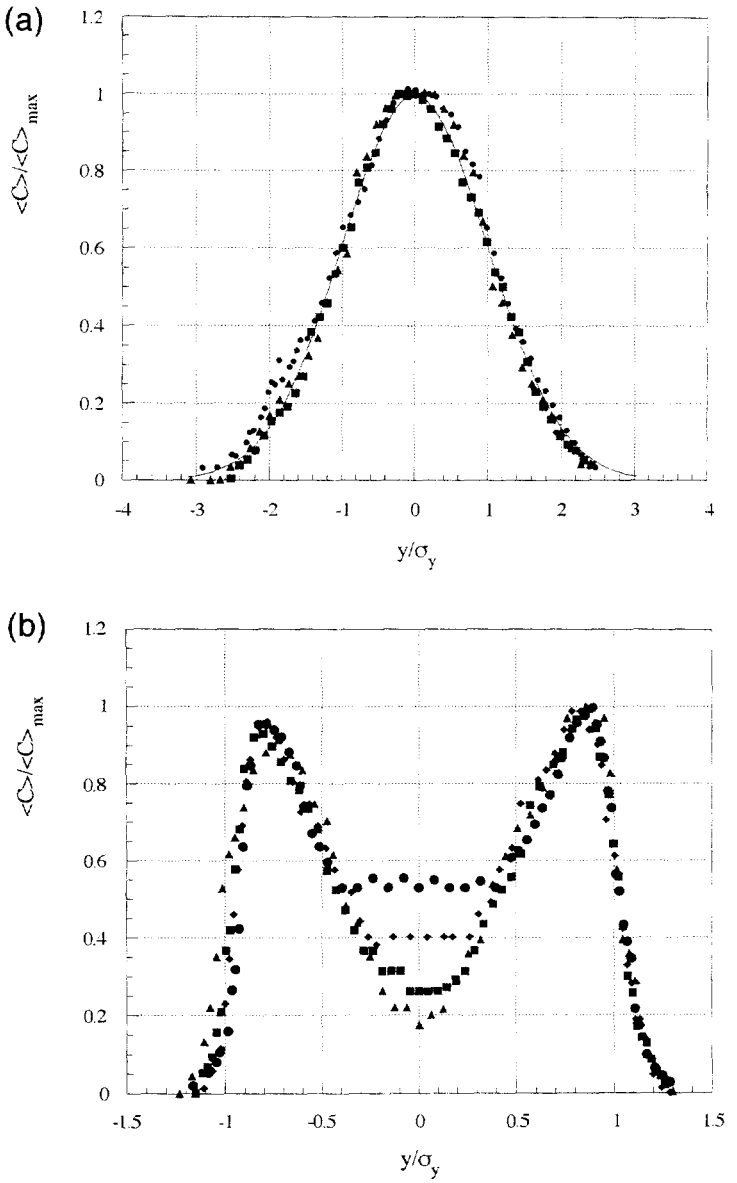

Fig. 4. Mean concentration profiles in the horizontal plane on flat floor. (a) Passive plumes; (b) dense plumes. Triangles refer to the section $X = 300$ mm, squares to 500 mm, inclined squares to 600 mm and circles to 800 mm. The line represents the gaussian curve

$$\frac{\langle C\rangle}{\langle C\rangle_{\max}} = \exp\left\{-\frac{1}{2}\left(\frac{y}{\sigma_y}\right)^2\right\}.$$

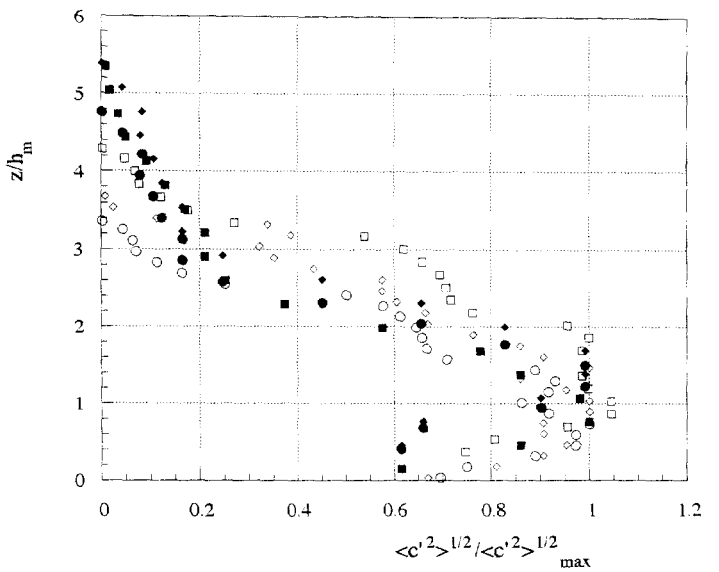

Fig. 5. Vertical r.m.s. concentration profiles for passive (open symbols) and dense (filled symbols) on flat floor in different sections (symbols as in Fig. 5).

mean reattachment is of order of $6H$ or $7H$. If we assume that H is much smaller than the boundary layer thickness $\delta(H \ll \delta)$, following Counihan et al., downstream of the fence, the wake can be divided into three regions, the wall and medium regions where the velocity deficit is greatest and the change in shear stress important and an external region where no modifications can be considered. A solid fence provides a flow of low turbulence in the near-wake zone. In the far wake region, at a distance of about $8H$, the mean velocity defects and excess turbulent stress profiles can be represented by functional forms and these quantities are decaying downstream as x^{-1} [19].

When a three-dimensional plume approaches a two-dimensional fence, the plume is blocked by the fence, widens upstream, and grows taller to surmount the fence with very marked dilution in the lee as seen in Fig. 6. These figures represent instantaneous images of passive and dense plumes jumping over the two-dimensional fence in the vertical plane (Fig. 6a and b) and the mean images of passive and dense plumes in both vertical and horizontal planes (Fig. 6c–f). We clearly see that the buoyancy effect amplifies the lateral width's increase which is finally controlled by the plume jumping the fence. The horizontal instantaneous and mean images exhibit the mainstream separation and the trailing vortices flow downstream, separation being always present downwind the 2D fence.

When considering dispersion problems, three parameters seem to be important for characterizing the flow over solid fences [6,20], the ratio H/h_{nf} of the fence height to the undisturbed plume height at the fence location, the Richardson number $R_{inf} = (g'_0 h_{nf})/(U_{nf}^2) = (g'_0 q_0)/(W_{nf} U_{nf}^3)$ where U_{nf} represents the advection (cross-section averaged) velocity of the plume and the ratio h_{nf}/W_{nf} of the undisturbed plume height to the undisturbed plume width at the fence location.

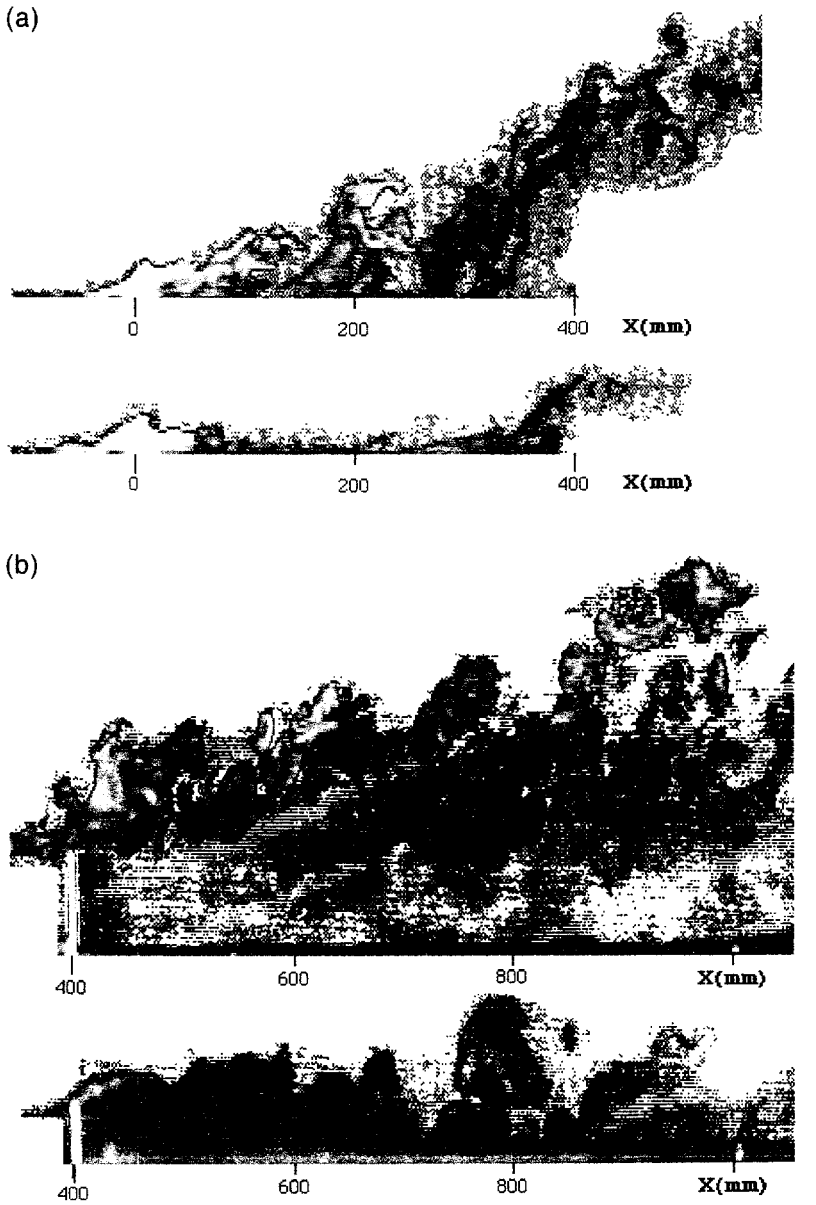

Fig. 6. Images upwind and downwind the 2D fence in the vertical and horizontal planes (up passive plumes, down dense plumes). (a) Instantaneous image upwind the fence; (b) instantaneous image downwind the fence; (c) mean image upwind the fence; (d) mean image downwind the fence; (e) mean image in the horizontal plane for passive plumes; (f) mean image in the horizontal plane for dense plumes.

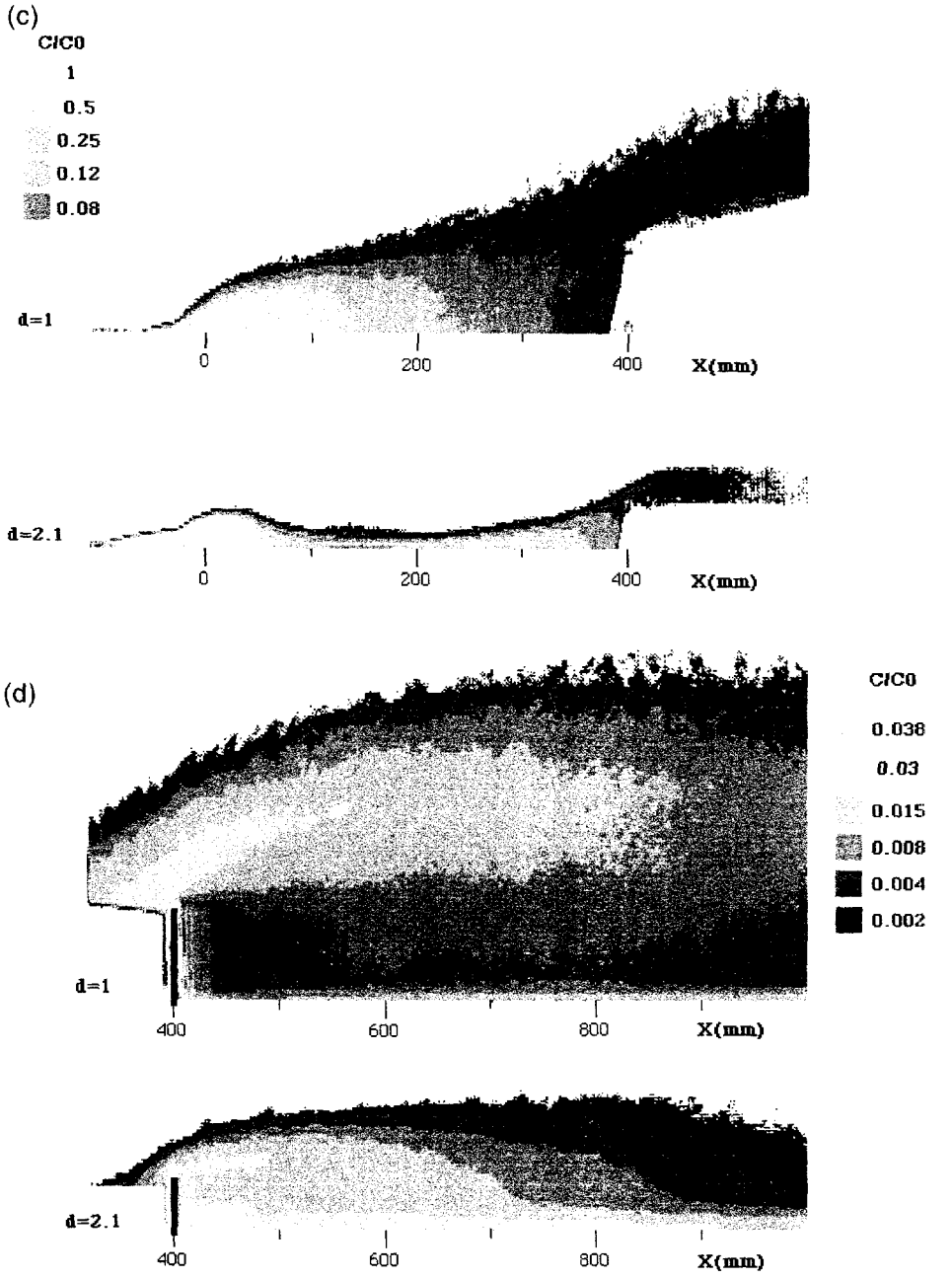

Fig. 6. (continued)

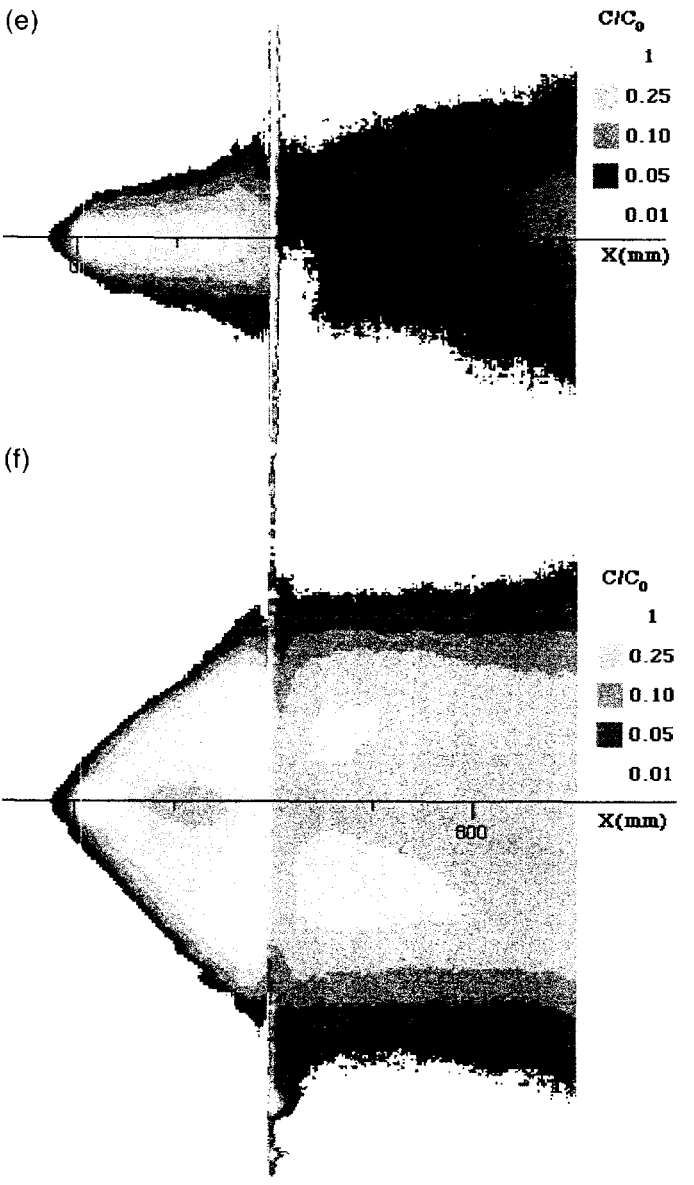

Fig. 6. (continued)

It seems that plume dilution is more strongly affected by the ratio of the obstacle height to the plume height than by the other parameters. When the fence is large compared to the plume depth, the first parameter greater than about 0.5, we can note a

large dilution of the plume downstream of the fence due to the turbulence in the wake and the width increase, mixing is as if the flow was passive in the lee of the fence. On the other hand, when the ratio is less than 0.5, there is little effect on the dispersion, only a small reduction in concentration caused by the obstacle is observed. For the neutral plumes and a 30-mm height fence in our experiments, this ratio was equal to 0.36 so that concentrations in the wake were of the same order of magnitude as passive plumes without obstacle. In this case, the fence had only small effects on the dilution. For this reason, we study different two-dimensional obstacles for the passive and the dense plumes. We decided to study solid fences of heights 60 mm and 30 mm, respectively, the ratio H/h_{nf} being 0.71 for passive and 1.3 for dense plumes.

3.3. Geometrical characteristics

One can define two different characteristic plume depths from the mean images. A visual depth h (or width W) could first be defined on the images by the threshold where no signal is recorded. We can see in Fig. 7a the evolutions of the visual plume height differences ($h_{obst} - h_{flat}$) between the plume's heights for flows over the obstacle and on flat floor and on Fig. 7b the same evolutions of the width differences ($W_{obst} - W_{flat}$) for the different densities and fences used. The effects of the 2D fences are clearly shown, the plume depths and widths being strongly influenced by buoyancy or stability. In front of the fences, plume heights are unchanged up to $X = 200$ mm and then grow in order to surmount the fences. We can note that both upwind and downwind the fences, the mean heights increase approximately linearly, the slopes are different upwind and downwind and the increase is more important for the semi-circular fence. On the other hand, the relative widths are of the same order of magnitude but the mean widths are larger downwind the fence than upwind as clearly seen in Fig. 6. It is quite interesting to note that just behind the 2D fence, the ratio W_f/W_{nf} for the mean plumes has nearly the same value, 1.93 and 1.99 for both passive and dense plumes which could mean that this fence has globally the same effect on the different plumes.

One can also compute an average height h_m defined by

$$\left\{\int_0^\infty \frac{\langle \rho(z)\rangle - \rho_a}{\rho_a} \mathrm{d}z\right\} h_m = \int_0^\infty \frac{\langle \rho(z)\rangle - \rho_a}{\rho_a} z \mathrm{d}z$$

These average heights h_m correspond to the ratio of the two first moments about ground level

$$h_m = \frac{\int_0^\infty z\langle C(z)\rangle \mathrm{d}z}{\int_0^\infty \langle C(z)\rangle \mathrm{d}z}$$

As reported in Fig. 8, the effects of the fences are much more important for dense plumes than for passive. In the fence section, the average heights increased more than two times greater for dense plumes. Associated with the increase in width, this could explain part of the major dilution of dense plumes.

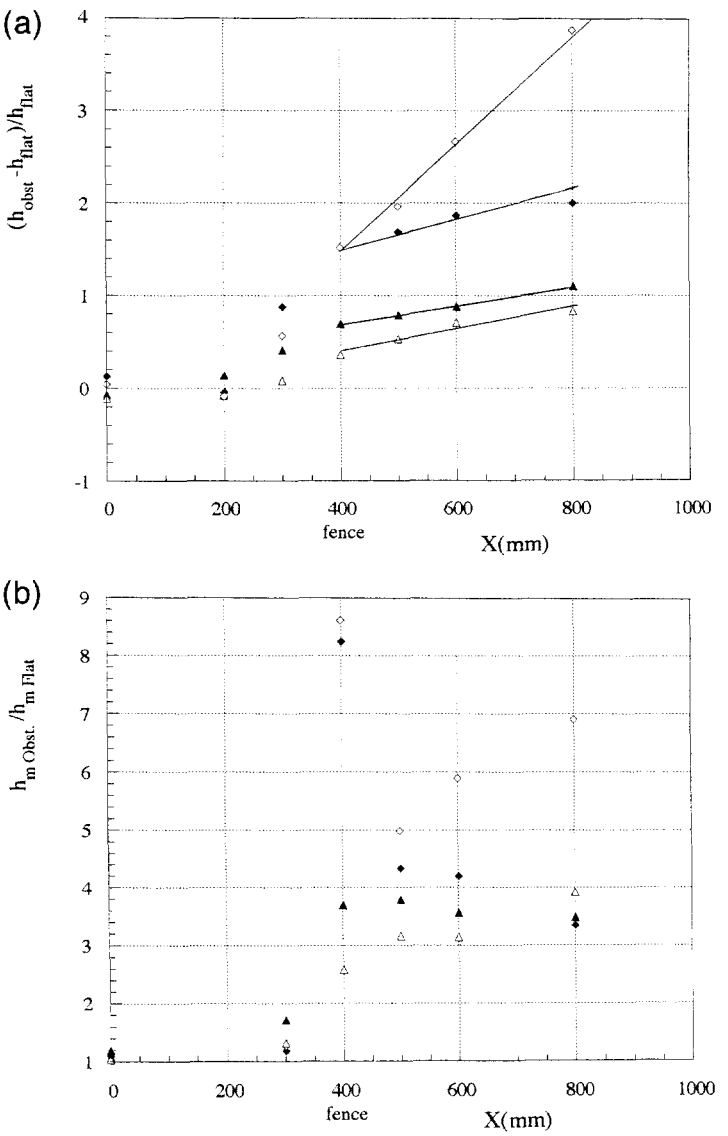

Fig. 7. Evolution of the heights plumes over the 2D (filled symbols) and semi-circular (open symbols) fences. (a) passive plumes (b) dense plumes. Triangles refer to passive plumes and squares to dense plumes.

3.4. Concentration characteristics

We present here some results concerning the dispersion over the two-dimensional fence as mean concentration, root-mean-square fluctuations, skewness and kurtosis, additional results concerning the semi-circular fence will also be given.

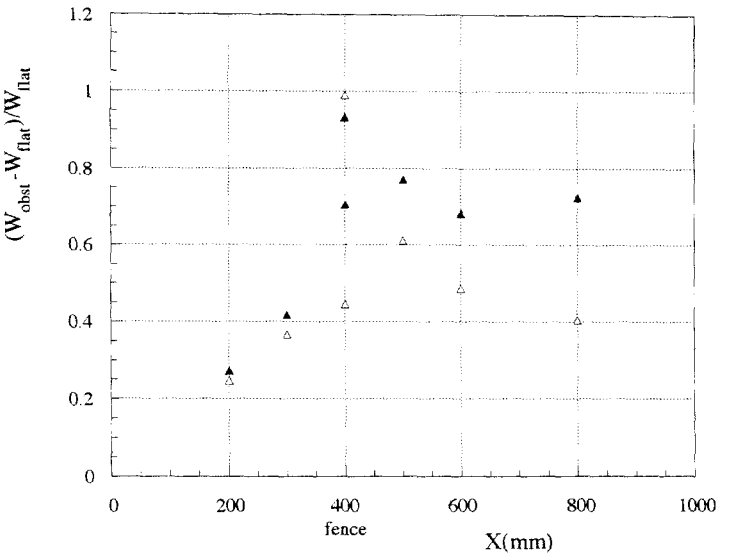

Fig. 8. Average heights h_m normalized by the relative average heights over flat floor for passive and dense mean plumes over 2D and semi-circular fences (symbols as in Fig. 7).

We can see in Fig. 9a the vertical mean concentration profiles $\langle C(x,0,z)\rangle$ normalized by the mean concentration at the source exit $\langle C_0(x_0,0,z_0)\rangle$ for the different releases at $X = 600$ mm, downwind the two types of fences. This section is situated just behind the downwind recirculation bubble for the dense plumes flowing over the 30-mm height fence. Dilution of dense plumes is very marked and is as if they were neutral, except near the ground level where concentration is maximum but no more than 4% of the initial concentration value. For the passive release, the mean plume concentration is clearly above the recirculation bubble and disperses in a classical way, profiles being in a gaussian form, maxima being in the wake. However, for dense gases, buoyancy affects dispersion in a different way. The dense gas slumps down to the ground as it passes over the recirculation bubble and recirculates back into the bubble. On the opposite way, we could expect the dense gas doesn't entrain immediately in the recirculation bubble downwind the fence. More, the dense gas passes over the fence in discrete patches.

When we compare the mean concentration in the horizontal plane as plotted in Fig. 9b for the same section, we could understand that dispersion downwind the 2D fence is greater than for the semi-circular only on the flow axis, a consequence of the buoyancy effects due to the great initial density (note that for passive plume and fence $H = 60$ mm, the horizontal light sheet is under the plume downwind the fence which explains the very small values). We can note that in the horizontal plane, the effects of the mainstream flow separation are important on the mean concentration but disappeared in the lee of the semi-circular fence. In that case, dense gas accumulates in front of the fence, inside the semi-cylinder and then rises over the fence, the rise being higher and dilution greater than with the two-dimensional fence. The two peaks disappear and we get again gaussian forms as dispersion on flat floor (Fig. 9b).

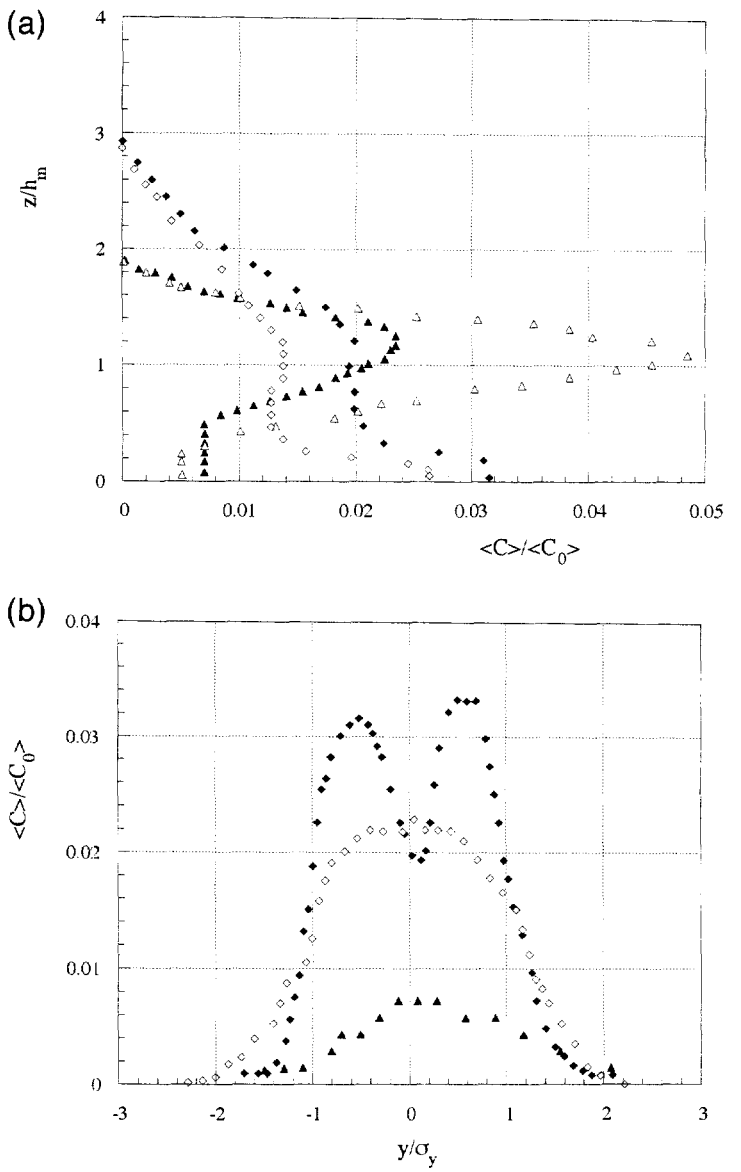

Fig. 9. Comparison of the mean concentration profiles for passive and dense plumes downwind the fences in the section $X = 600$ mm. (a) Vertical profiles; (b) horizontal profiles. Triangles refer to passive plumes, squares to dense plumes, filled symbols to flow over the 2D fence and open symbols to flow over the semi-circular fence.

When normalized by the maximum of concentration in each section and by the averaged height h_m for the vertical profiles (Fig. 10a) and by the plume width σ_y for the horizontal profiles (Fig. 10b), the different profiles are all similar and some

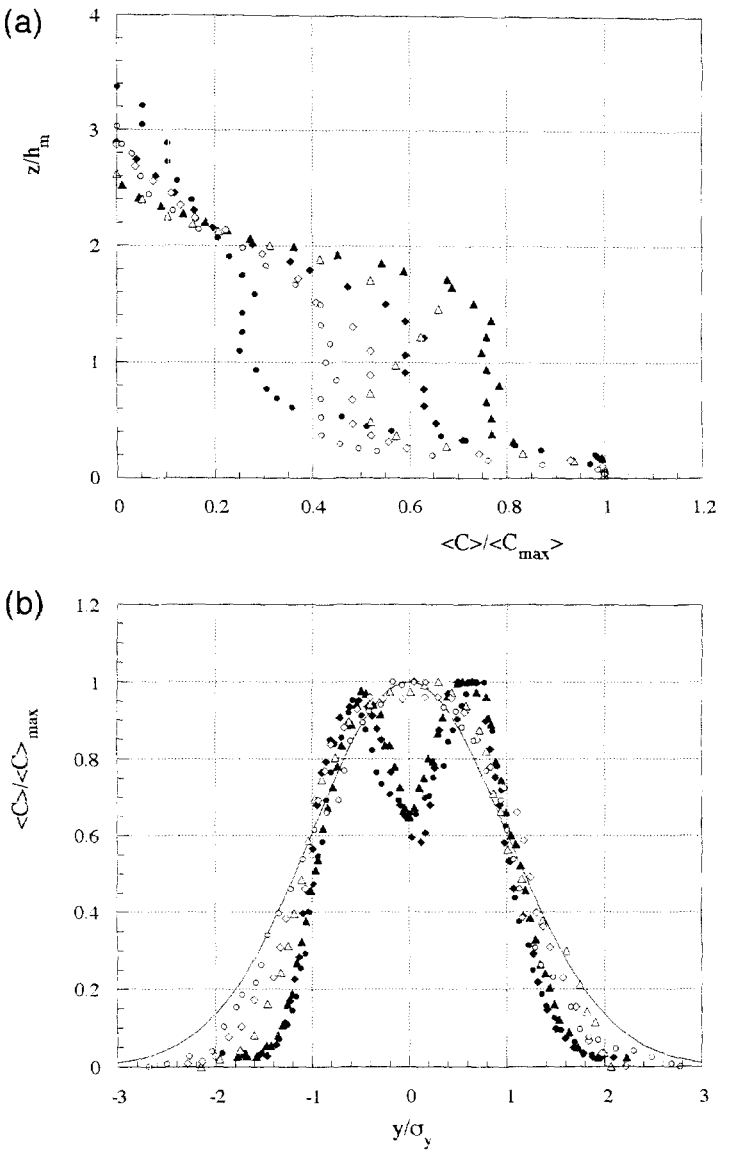

Fig. 10. Normalized mean concentration downwind the 2D (open symbols) and semi-circular (filled symbols) fences for the dense plumes. (a) Vertical profiles; (b) horizontal profiles. Triangles refer to the section $X = 500$ mm, squares to 600 mm and circles to 800 mm. The line represents the gaussian curve.

self-similarity could be expressed, at least in the horizontal plane. The effects of the mainstream separation flow by the dense release are strongly marked as clearly seen in front of both obstacles (Fig. 6). Downstream the 2D fence, the mean horizontal concentration profiles still exhibit two peaks on the two sides of the axis for the different

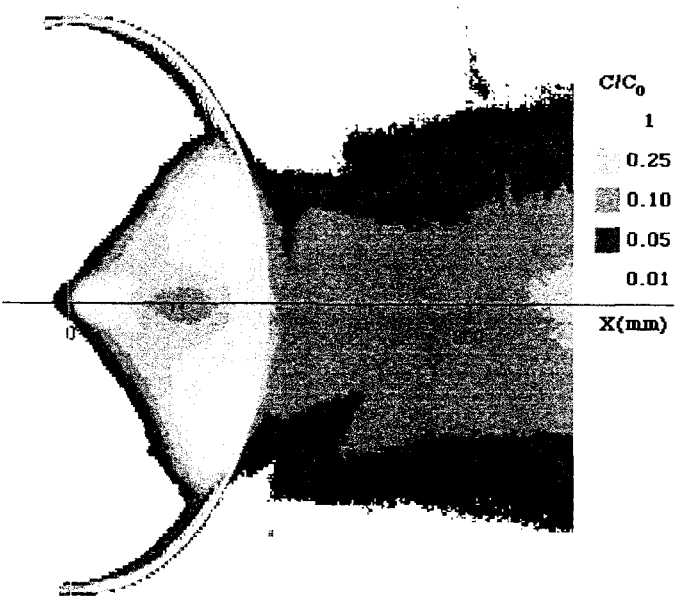

Fig. 11. Mean concentration image for dense plumes downwind the semi-circular fence in the horizontal plane.

sections (Fig. 10b). Otherwise, downwind the semi-circular fence, the effect of the separation flow disappears downwind (Fig. 11) and all mean concentration profiles exhibit some gaussian form (Fig. 10b).

One can also determine the non-dimensionalized mean concentration differences between obstacle and flat terrain

$$\frac{\Delta\langle C\rangle}{\langle C_0\rangle} = \frac{\langle C\rangle_{\text{fence}}}{\langle C_0\rangle} - \frac{\langle C\rangle_{\text{flat}}}{\langle C_0\rangle}$$

They are plotted on Figs. 12 and 13 for neutral and dense plumes in the vertical and horizontal planes for dense plume. They exhibit the effects of obstacles on the different plumes and have the same global aspect. For example, all the horizontal differences for the mean dense plume over the 2D fence are negatives, mean concentration downwind the 2D obstacle being everywhere lower than without obstacle in the plane of visualization, the maximum being for $y = \sigma_y$. This phenomena is amplified by the semi-circular fence due to the greater height of the mean plume.

Fig. 14 represents the vertical profiles of the ratio of the root-mean-square fluctuations to the initial mean concentration for these two neutral and dense plumes downwind the obstacles and in one section, $X = 600$ mm. Values for dense plumes are very much smaller than for passive, a consequence of the stratification. When normalized by the local mean values as shown in Fig. 15a in the vertical plane, all these profiles are shape similar in the different sections with higher values at the outer edge of the plumes where mixing is intense and mean values small. A tendency to self-similarity is observed in both horizontal and vertical plane. Fig. 15b represents the r.m.s. fluctuations normalized

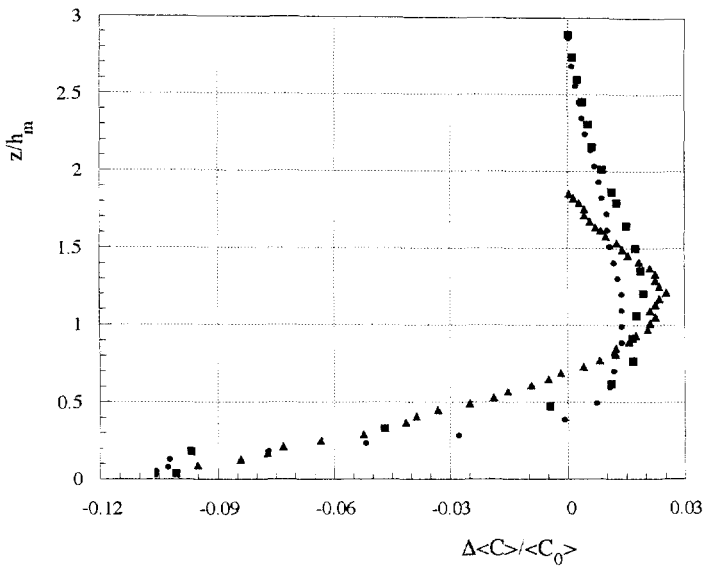

Fig. 12. Vertical mean concentration differences profiles between the dispersion over fences and on flat floor in the section $X = 600$ mm for the dense plumes over the 2D fence. Triangles refer to passive plumes over 2D fence, squares to dense plumes over 2D fence and circles to dense plumes over circular fence.

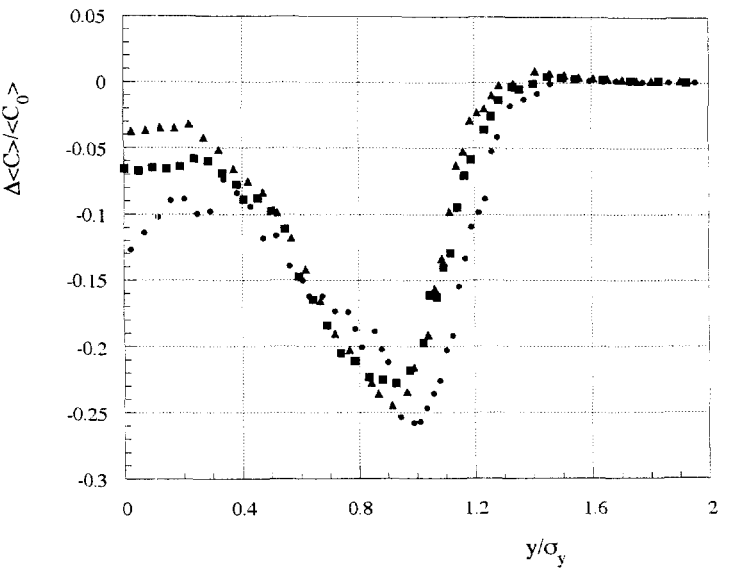

Fig. 13. Horizontal mean concentration differences profiles between the dispersion over fences and on flat floor for the dense plumes over the 2D fence. Triangles refer to the section $X = 500$ mm, squares to 600 mm and circles to 800 mm.

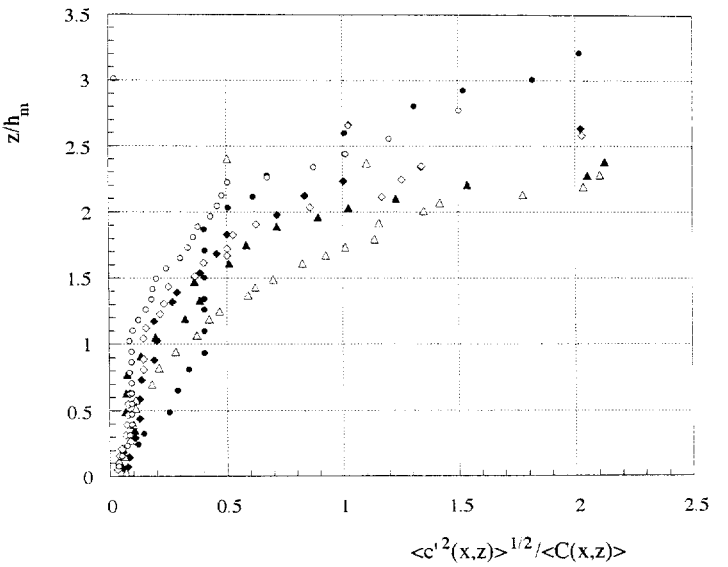

Fig. 14. R.m.s. concentration profiles for the passive and dense plumes downwind the 2D and semi-circular fences in the vertical plane (symbols as in Fig. 10).

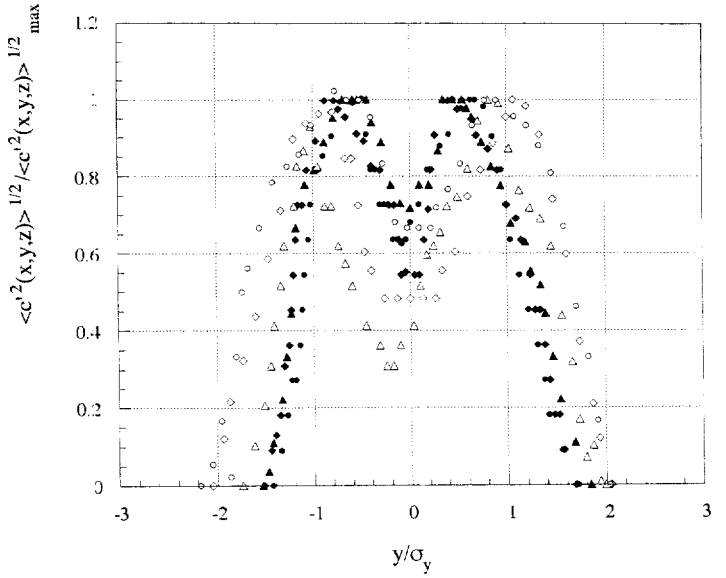

Fig. 15. R.m.s. concentration profiles for the dense plumes downwind the 2D and semi-circular fences. (a) Vertical; (b) horizontal (symbols as in Fig. 11).

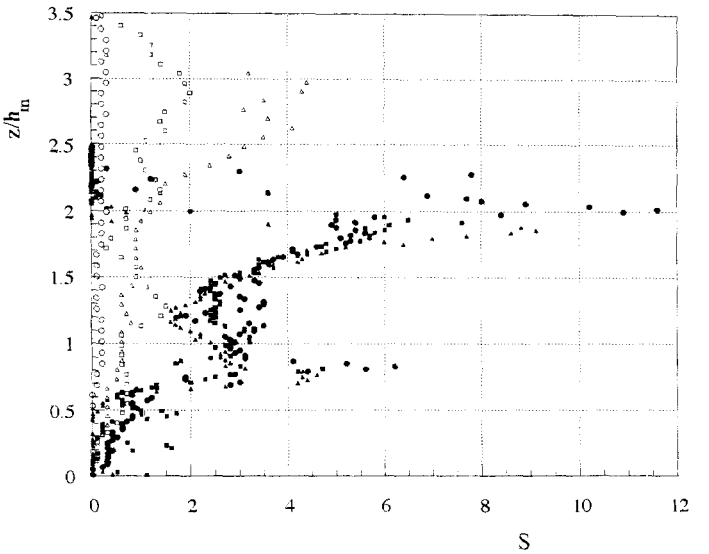

Fig. 16. Vertical skewness concentration profiles downwind the 2D fence for passive (filled symbols) and dense (open symbols) plumes. Triangles refer to the section $X = 500$ mm, squares to 600 mm and circles to 800 mm.

by the maximum value in each section in the horizontal plane. For both obstacles, the r.m.s. fluctuations are affected by vortices although, for mean concentration in the lee of the semi-circular fence, these effects were not present.

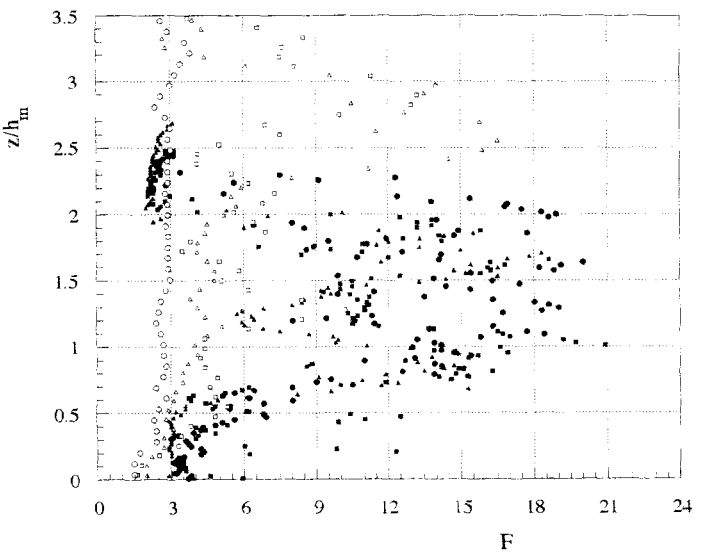

Fig. 17. Vertical flatness concentration profiles downwind the 2D fence for passive (filled symbols) and dense (open symbols) plumes (symbols as in Fig. 16).

Skewness and kurtosis vertical profiles are shown in Figs. 16 and 17 for passive and dense plumes downwind the 2D fence. It is evident that the effect of buoyancy is to reduce these values relative to passive scalar, smaller values are obtained close to the surface and greater values near the boundaries. We could note a tendency for the dense plumes characteristics towards gaussian values when going downstream.

4. Conclusion

The light scattering properties of small particles have been used to study the effects of two-dimensional obstacles on the dispersion of continuous dense gas releases. The general framework of the experimental technique using flow visualization and image processing was described. Quantitative statistical results of the dispersion of continuous releases has been presented.

The effects of negative buoyancy are clearly shown. For dense plumes, dilution downwind of the two fences studied is as if the flow was passive. The relative height differences are very much greater when the relative widths are of the same order of magnitude. Some self-similarity could be expected for mean concentration and root-mean-square fluctuations normalized by their maxima in both horizontal and vertical planes, the vertical and horizontal distances being normalized with the average height h_m and the plume width σ_y. On the other hand, the root-mean-square concentration fluctuations concentration are much lower for dense plumes than for neutral ones and all profiles look similar for the different fences studied. More, an effect of buoyancy is to tend towards gaussian values for skewness and kurtosis.

The fence's shape seems also to be an important parameter, the downstream vortices flow, an effect of the negative buoyancy on the external flow, is a good example of the influence of the shape on dispersion.

Acknowledgements

The work presented here was done as part of the 'STEP' programme of the Commission of the European Communities and was also partially supported by METRAFLU.

References

[1] J.S. Puttock, Stably stratified flow and dense gas dispersion, Oxford, Clarendon.
[2] R.E. Britter, Atmospheric dispersion of dense gases, Ann. Rev. FL Mech. (1989b) 317–344.
[3] J. McQuaid, in: J. McQuaid (Ed.), Heavy Gas Dispersion Trials at Thorney Island, Elsevier, 1985.
[4] G. Ooms, H. Tennekes, in: G. Ooms, H. Tennekes (Eds.), Atmospheric Dispersion of Heavy Gases and Small Particles, Springer-Verlag, 1984.
[5] R.E. Britter, McQuaid, Workbook on the dispersion of dense gases, Health Saf. Exec. Rep. Sheffield, UK, 1988.
[6] R.E. Britter, Experiments on some effects of obstacles on dense gas dispersion, AEA Report SRD R 407, 1989a.

[7] D.J. Hall, R.A. Waters, Investigation of two features of continuously released heavy gas plumes, Warren Spring Laboratory Report LR 707, 1989.
[8] M. Schatzmann, W.H. Snyder, R.E. Lawson Jr., Experiments with heavy gas jets in laminar and turbulent cross-flows, Atmos. Environ. 27A (7) (1993) 1105–1116.
[9] Builtjes, 1984.
[10] S.B. Sutton, H. Brandt, B.R. White, Atmospheric dispersion of a heavier-than-air gas near a two-dimensional obstacle, Boundary-Layer Meteorology 35 (1986) 125–153.
[11] Fladis final report, Research on the dispersion of two-phase flashing releases, E.C., DG XII, 1994.
[12] M. Ayrault, S. Simoëns, Turbulent concentration determination in gas flow using multiple CCD cameras, J. Flow Visualiz. Image Process. 2 (1995) .
[13] M. Ayrault, J.L. Balint, R. Morel, An experimental study on the evolution and dispersion of a cloud of gas heavier than air, J. Haza. Mater. 26 (1991) 1–26.
[14] G.T. Csanady, Turbulent diffusion in the environment, Reidel, 1972.
[15] M. Ayrault, Fladis Report, CEE, 1994.
[16] R.E. Britter, W. Snyder, Fluid modelling of dense gas dispersion over a ramp, J. Haza. Mater. 18 (1988) 37–67.
[17] D. Stretch, The dispersion of slightly dense contaminant, PhD Thesis, Cambridge, England, 1986.
[18] J. Counihan, J.C.R. Hunt, P.S. Jackson, Wakes behind two-dimensional surface obstacles, J. Fluid Mech. 64 (1974) 529–563.
[19] M.D. Perera, Shelter behind two-dimensional solid and porous fences, J. Wind Eng. Ind. Aerodyn. 8 (1981) 93–104.
[20] S.J. Jones, D.M. Webber, The interaction of a dense gas plume with a fence, Trans. IChemE. 71 (1993) .